Gentle Driving of Piles at a Sandy Site Combining Axial and Torsional Vibrations Quantifying the Influence of Pile Installation Method on Lateral Behavior

Kementzetzidis, Evangelos; Pisanò, Federico; Tsetas, Athanasios; Metrikine, Andrei V.

DOI
10.1061/JGGEFK.GTENG-11179

Publication date
2023

Document Version
Final published version

Published in
Journal of Geotechnical and Geoenvironmental Engineering

Citation (APA)
Kementzetzidis, E., Pisanò, F., Tsetas, A., & Metrikine, A. V. (2023). Gentle Driving of Piles at a Sandy Site Combining Axial and Torsional Vibrations: Quantifying the Influence of Pile Installation Method on Lateral Behavior. *Journal of Geotechnical and Geoenvironmental Engineering*, *149*(11), Article 04023102. https://doi.org/10.1061/JGGEFK.GTENG-11179

Gentle Driving of Piles at a Sandy Site Combining Axial and Torsional Vibrations: Quantifying the Influence of Pile Installation Method on Lateral Behavior

Evangelos Kementzetzidis[1]; Federico Pisanò[2]; Athanasios Tsetas[3]; and Andrei V. Metrikine[4]

Abstract: Gentle driving of piles (GDP) is a new technology for the vibratory installation of tubular (mono) piles that aims to achieve both efficient installation and low noise emission by combining axial and torsional vibrations. To provide a preliminary demonstration of the GDP concept, onshore medium-scale tests in sand were performed in late 2019 at the Maasvlakte II site in Rotterdam (Netherlands). Several piles were installed using both impact and vibratory driving methods (including GDP), with the twofold aim of comparatively assessing (1) the effectiveness of GDP; and (2) the presence of installation effects in the pile response to lateral loading. This work focuses on the latter aspect and presents a quantitative analysis of the installation effects observed in the pile loading test data recorded in the field. Due to soil inhomogeneity across the field, a purely data-based analysis would have not supported objective conclusions, which led to adoption of an alternative approach based on one-dimensional (1D) numerical modeling. To this end, an advanced cyclic p–y model was calibrated for the simulation of the reference pile loading tests, and the values of key parameters were compared to infer quantitative information about relevant installation effects. The results presented herein inform about the promising performance of the GDP method, particularly in comparison to traditional impact hammering. Although the cyclic lateral pile behavior proves affected by the installation process, certain important aspects of installation effects gradually diminish as more loading cycles are applied. **DOI: 10.1061/JGGEFK.GTENG-11179.**

Introduction

Since the installation in 1991 of the first 5-MW offshore wind farm in Denmark, over 28 GW of offshore wind power have been developed in Europe (Komusanac et al. 2022), while a global capacity of 37 GW was reported at the end of 2021 (Lee et al. 2021). In the coming 30 years, North America, Europe, and Asia will lead the way toward the installation of additional 560 GW, which is likely a lower-bound estimate of the real growth that will take place (Lee et al. 2021). To support this unprecedented energy transition endeavor, considerable research efforts are being devoted to closing knowledge gaps and promoting innovation in all areas of offshore wind science and engineering. Among many others, such areas include the installation (and future decommissioning) of ever larger offshore wind turbines (OWTs), which are currently approaching and exceeding a power output of 15 MW (Gaertner et al. 2020). Therefore, the remarkable fabrication costs for these enormous steel structures may only be alleviated by optimizing the design of the whole OWT-foundation system, particularly with respect to environmental cyclic loading conditions (Igwemezie et al. 2019; Byrne et al. 2020a; Pisanò et al. 2022).

To date, OWTs are most often founded on so-called monopiles, which are tubular steel piles featuring a large diameter (in the range from 5 to 11 m) and a low ratio between embedded length and diameter (typically between 3 and 6). Monopiles are most commonly installed through impact hammering, a technology that has substantially matured over years of intense offshore oil and gas developments (Kallehave et al. 2015). However, while impact installation may sometimes slow down (or even abort) in the presence of very competent soils (Rodger and Littlejohn 1980; Achmus et al. 2020), its execution inevitably produces significant underwater noise. Because such noise is known to be harmful to marine life, ocean management authorities have been enforcing strict regulations to limit its negative impact on the environment (Tsouvalas 2020). A promising, less noisy alternative to impact piling is represented by vibratory pile-driving technologies: their performance in different soil types, as well as their impact on postinstallation pile behavior, is being investigated by an increasing number of research teams (LeBlanc 2014; Herwig and Gattermann 2015; Heins and Grabe 2017; Labenski and Moormann 2019; Anusic et al. 2019; Achmus et al. 2020; Staubach et al. 2022; Tsetas et al. 2023b).

This study presents some recent achievements related to the development and assessment of a new vibratory pile installation technology named gentle driving of piles (GDP) (Metrikine et al. 2020). The GDP method replaces the high-amplitude blows of traditional impact hammering with axial and torsional vibrations, with the latter applied at a substantially higher frequency than the former. The first demonstration of the GDP technology has been recently accomplished through a field campaign at the Maasvlakte II site in Rotterdam (Netherlands). To enable a general comparison among different pile installation methods, identical tubular test piles (see specifications in Table 1) were installed in sandy soil using three different driving technologies, namely, impact hammering,

[1]Assistant Professor, Faculty of Civil Engineering and Geosciences, Delft Univ. of Technology, Delft 2628 CN, Netherlands. ORCID: https://orcid.org/0000-0002-4426-1072. Email: e.kementzetzidis@tudelft.nl

[2]Associate Professor, Faculty of Civil Engineering and Geosciences, Delft Univ. of Technology, Delft 2628 CN, Netherlands (corresponding author). Email: f.pisano@tudelft.nl

[3]Postdoctoral Researcher, Faculty of Civil Engineering and Geosciences, Delft Univ. of Technology, Delft 2628 CN, Netherlands. ORCID: https://orcid.org/0000-0003-1712-3376. Email: a.tsetas@tudelft.nl

[4]Professor, Faculty of Civil Engineering and Geosciences, Delft Univ. of Technology, Delft 2628 CN, Netherlands. Email: a.metrikine@tudelft.nl

Note. This manuscript was submitted on July 12, 2022; approved on April 25, 2023; published online on September 4, 2023. Discussion period open until February 4, 2024; separate discussions must be submitted for individual papers. This paper is part of the ***Journal of Geotechnical and Geoenvironmental Engineering***, © ASCE, ISSN 1090-0241.

Table 1. Geometrical specifications of the test and reaction piles

Pile geometry	Symbol	Test piles	Reaction pile
Length (m)	L	10	10
Embedded length (m)	L_e	8	8
Outer diameter (m)	D	0.762	1.6
Wall thickness (m)	h	0.0159	0.02

traditional axial vibratory piling, and the new GDP method (Tsetas et al. 2023a); subsequently, the same piles were subjected to lateral cyclic load parcels of varying amplitude, so as to enable a first assessment of GDP installation effects in comparison to existing technologies (Kementzetzidis et al. 2023). Additionally, complementary pile impact tests were also performed to confirm (or challenge) certain indications provided by the main cyclic loading experiments.

Regarding the postinstallation cyclic tests, the inhomogeneity of the site and the location of the water table (about 4 m below the ground surface) had altogether a noticeable impact on the cyclic response of the test piles—largely due to the occurrence of pile–soil gapping in the shallow unsaturated sand. Although onshore site effects are also clearly visible in previously published field data (Li et al. 2015; Byrne et al. 2020b; Prendergast and Igoe 2022), a model-based analysis of the GDP cyclic test results was carried out in this work to try and decipher relevant installation effects in the lateral response of the test piles. To this end, the cyclic soil reaction model recently proposed by Kementzetzidis et al. (2022) was adopted to simulate cyclic ratcheting and gapping effects as observed at the Maasvlakte II site. Following a calibration of the model parameters largely based on seismic cone penetration test (SCPTu) data, the proposed analysis provides encouraging evidence regarding the lateral behavior of GDP-driven piles.

Field Tests at the Maasvlakte II Site

All GDP field tests were performed at the Maasvlakte II port site in Rotterdam, Netherlands, which comprises the North Sea sand that was used to create a reclaimed and compacted site. The experimental campaign was carried out over 6 months (June to December 2019) and included the execution of geotechnical site investigation, pile installation experiments, and cyclic lateral loading tests, with the addition of the aforementioned pile impact tests. After the conclusion of site investigation activities, nine tubular steel piles were installed at the test site in October and November 2019, namely, eight test piles and one larger reaction pile (the latter to serve as a central fixed point for the postinstallation loading tests; Table 1). Four of the test piles, henceforth referred to as main test piles (MTPs), were extensively instrumented as reported by Tsetas et al. (2023a); the other four auxiliary test piles (ATPs) were installed uninstrumented for preliminary testing purposes. The remainder of this paper exclusively focuses on analyzing the behavior of the four MTPs, which were labeled after the corresponding installation method: IH (impact hammering), VH (axial vibro-hammering), and $GDP_{1,2}$ (two MTPs were GDP-driven).

Geotechnical Site Investigation

Geotechnical investigation activities took place at the Maasvlakte II site between June and August 2019. A preliminary phase of site investigation was first carried out in June 2019 to support the selection of the test pile locations. To this end, 25 cone penetration test with pore water pressure measurement (CPTu) tests were performed down to a target depth of 10 m, which also enabled the identification of the water table depth—on average, approximately 4 m below the ground surface. A more detailed site investigation program was executed 2 months later, including the following tests at the MTP locations:

- Four SCPTu tests: see Fig. 1;
- Four hydro-profiling tests with minipump tests (HPT-MPT) around the piles (target depth = 15 m); and
- Borehole sampling around the piles, with a total of eight 10-m-long boreholes (two per MTP)—resulting soil classification information was provided by Tsetas et al. (2023a).

The main outcomes of the SCPTu tests are summarized in Fig. 1. The profiles of cone resistance (q_c), relative density [D_r obtained following Jamiolkowski et al. (2003)], and shear wave velocity (V_s) indicate somewhat inhomogeneous sand conditions, featuring a negative D_r gradient below a depth of approximately 1 m. Importantly, the soil profile at the VH pile location was found to be quite different from that at the IH/$GDP_{1,2}$ locations, with significantly looser sand below the water table.

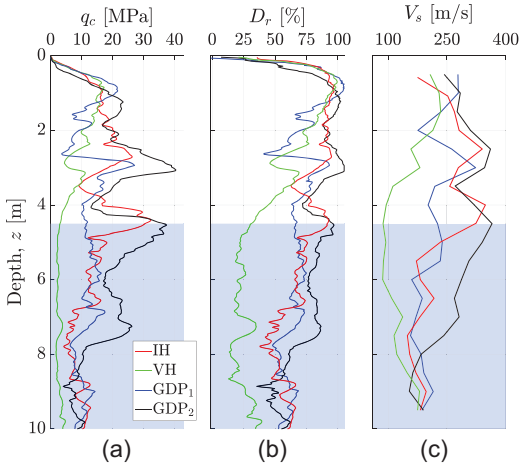

Fig. 1. (Color) Profiles of (a) cone resistance (q_c); (b) relative density (D_r); and (c) S-wave velocity (V_s) obtained at the MTP locations through in situ SCPTu tests. The shaded areas indicate water-saturated soil. (Adapted from Kementzetzidis et al. 2023.)

Installation of MTPs

During the first week of November 2019, all four MTPs were driven into the ground according to the following installation protocol: first, piles were driven down to a depth of 3 m, with each pile laterally restrained to ensure verticality; then the lateral restraints were removed and the piles were finally driven down to the target penetration depth of 8 m. The pile-driving settings are summarized in Table 2 for each MTP, while the consumed energy for the vibratory-installed piles is presented in Fig. 2. When considering the specific soil profiles in Fig. 1, the driving performance of the GDP method stands out both in terms of installation time and consumed energy to achieve the required target depth—comparing the driving records of piles GDP_1 and VH pile, the GDP-driven pile installed in a considerably more competent soil (Fig. 1) achieves the target depth faster, with almost equal energy consumption.

Cyclic Lateral Loading Tests

The lateral loading tests, the main subject of this paper, were performed using the loading frame shown in Fig. 3. Because all test piles were installed to a target depth of 8 m, the remaining pile length allowed lateral loading with an eccentricity $e = 1$ m above the

Table 2. Driving settings and duration associated with the main pile-driving phase ($z = 3 - 8$ m) for the four MTPs

Driving info	IH	VH	GDP_1	GDP_2
Driving settings	$E_b = 24.97$ kJ $N_b = 70$ blows/min	$me = 25$ kg · m $f_{ax} = 24.8$ Hz	Axial $me = 15$ kg · m $f_{ax} = 16.3$ Hz	Torsional $me = 4$ kg · m $f_{tor} = 63$ Hz
Driving duration	348 s	261 s	151 s	273 s

Note: E_b and N_b = energy per blow and number of blows per minute for IH pile; and me and f = eccentric moment and the driving frequency for the vibratory methods (both VH and GDP).

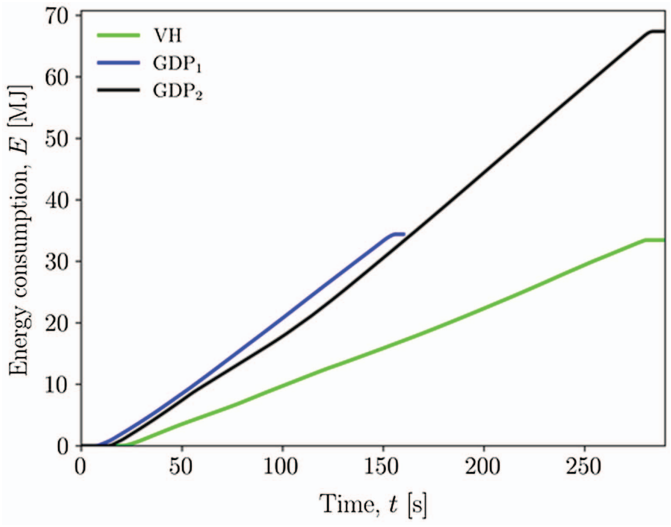

Fig. 2. (Color) Energy consumption over installation time during the final 5 m of pile driving (out of the total 8 m) for the axial and GDP vibro-driven piles.

ground surface. During lateral loading, the deflection of all test piles was sampled near the soil surface (shown in the following after low-pass filtering at 70 Hz) using dedicated displacement sensors (Gefran PY1, 100-mm stroke, Provaglio d'Iseo, Italy).

Fig. 4 illustrates the MTP loading program, featuring a combination of slow (cyclic) and faster (dynamic) load parcels. Cyclic parcels were applied with relatively large amplitude at a constant low frequency of 0.1 Hz (black parcels in Fig. 4) from a to e.; each cyclic parcel comprised $N = 1{,}000$ cycles, with a maximum applied load of 350 kN—an approximate reference lateral capacity of 1.5 MN was identified for the GDP-driven MTPs as a reasonable approximation (Kementzetzidis et al. 2023). The gray parcels in Fig. 4 represent dynamic load parcels, i.e., small-amplitude (5-kN) frequency sweeps interleaved between consecutive cyclic parcels. Each sweep was set to span loading frequencies ranging from 0.1 to 4 Hz to explore possible frequency-dependence features in the small-vibration response of the system (Kementzetzidis et al. 2021). Previous studies have shown that the dynamic response properties of offshore wind turbines can be considerably affected by the loading history (Kementzetzidis et al. 2018, 2019). In what follows, selected data from the GDP testing campaign are reported to summarize relevant features of MTPs' behavior.

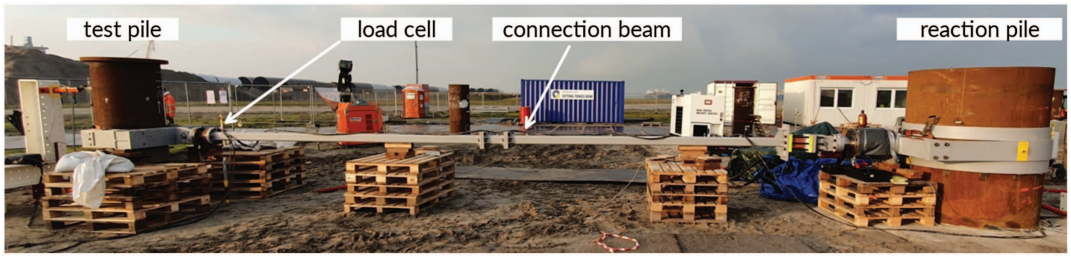

Fig. 3. (Color) Loading frame connecting a test pile to the reaction pile. [Reprinted from Kementzetzidis et al. (2023), under Creative Commons-4.0 International (https://creativecommons.org/licenses/by/4.0/).]

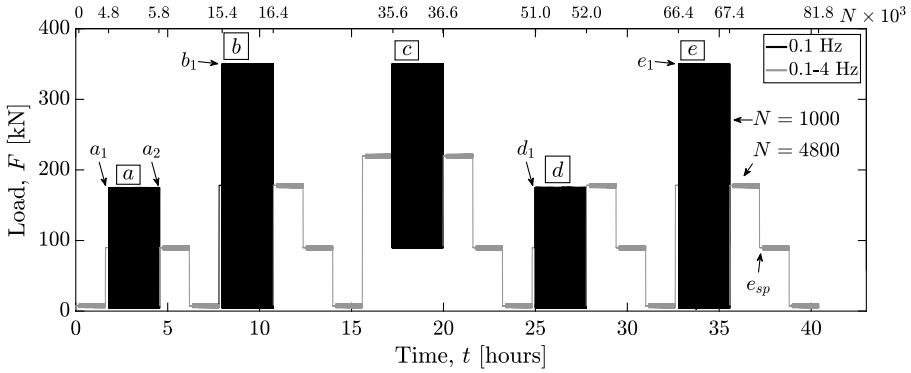

Fig. 4. Cyclic/dynamic loading program. Load amplitudes are provided against time (bottom axis) and number of cycles (top axis). Cyclic load parcels ($a - e$, $N = 1{,}000$ for each parcel) and dynamic frequency sweeps ($N = 4{,}800$ per sweep) are shown in black and gray, respectively. (Adapted from Kementzetzidis et al. 2023.)

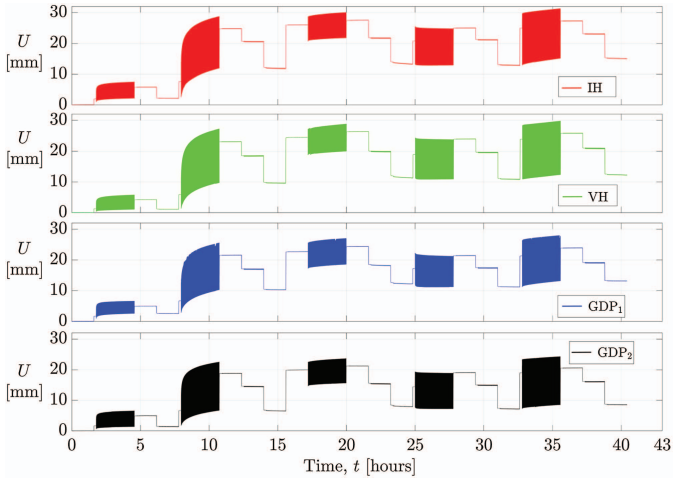

Fig. 5. (Color) Lateral deflection of all MTPs (soil surface level) under the loading program in Fig. 4.

Fig. 5 reports the evolution in time of the lateral deflection measured for all MTPs under the loading program in Fig. 4 (displacement values measured at the soil surface). Despite mild quantitative differences, all piles exhibited similar displacement accumulation patterns, with clear appearance of cyclic ratcheting behavior. Interestingly, all load parcels except d induced displacement responses characterized by positive accumulation rates, while a gradual reduction in accumulated deflection was observed during Parcel d. Such a mechanism, sometimes termed self-healing, stabilization, or relaxation, has been previously documented in relation to small-scale $1g$ tests on monopiles (Sturm et al. 2008; Theodoros et al. 2009). Fig. 5 also suggests that the low-amplitude frequency sweeps had negligible impact on the overall pile displacement trends. At the end of the loading program, the IH pile accumulated the most lateral deflection, followed by VH, GDP_1, and GDP_2, which may be also clearly observed in Fig. 6.

Fig. 6(a) shows the cyclic force–displacement response of all MTPs (displacement measured at the soil surface) to the whole

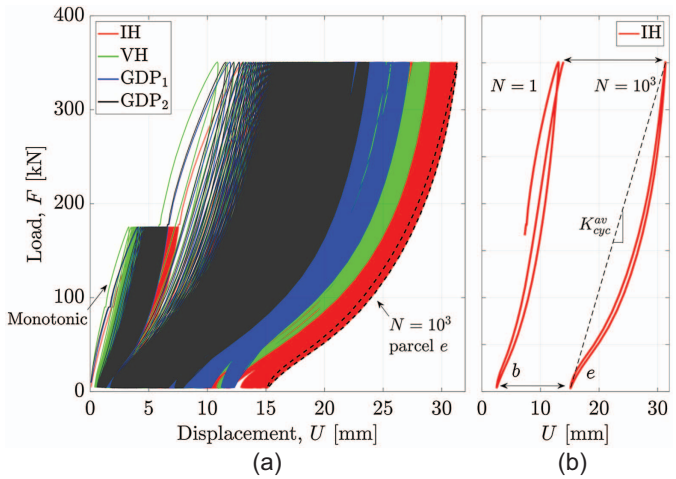

Fig. 6. (Color) (a) Force–displacement response of all MTPs (displacement measured at the soil surface) to the loading program in Fig. 4; the label "Monotonic" refers to the first loading branch in Parcel a; and (b) IH pile response to the first cycle ($N = 1$) in Parcel b and the last cycle ($N = 1{,}000$) in Parcel e, for which the definition of cyclic secant stiffness K_{cyc}^{av} is visualized.

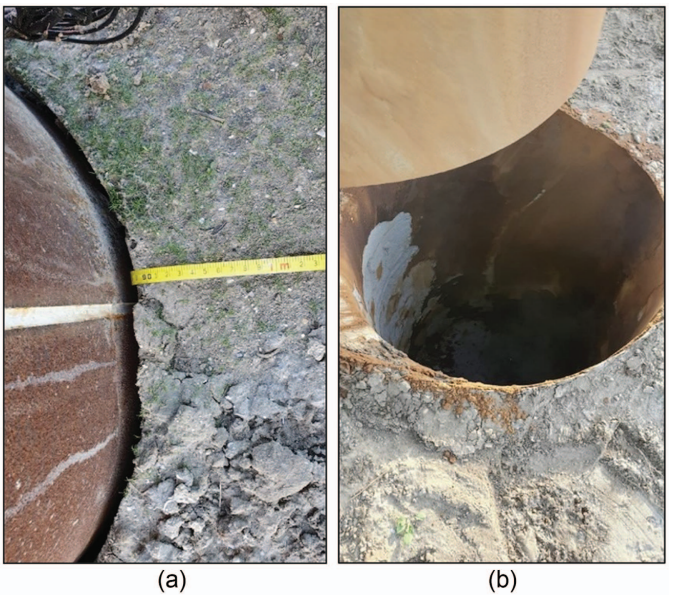

Fig. 7. (Color) Evidence of pile–soil gapping (a) at the end of the cyclic loading program; and (b) after pile extraction.

loading program in Fig. 4. The shape of the measured cyclic responses indicates the occurrence of pile–soil separation (gapping) during the loading tests, which was likely enabled by the hydraulic suction, and the resulting apparent cohesion in the shallow unsaturated sand above the water table (Fredlund 2006). This kind of response would not be expected for piles installed in either dry or fully saturated (uncemented) sand. The influence of gapping is more clearly illustrated in Fig. 6(b), which reports the response cycles measured for the IH pile under the first cycle ($N = 1$) of Parcel b and the last cycle ($N = 1{,}000$) of Parcel e (compare with Fig. 4): both the unloading and reloading branches of the response appear to be of a locking type, with the tangent lateral stiffness increasing with the load level. This is a well-known consequence of the pile–soil reengagement that occurs upon the gradual (re)closure of the gap (Kementzetzidis et al. 2023). Visual pile–soil inspection further confirmed the alleged impact of gapping in the shallow unsaturated soil: see the pictures in Fig. 7 associated with at rest (i.e., at the end of cycling) [Fig. 7(a)] and post-extraction conditions [Fig. 7(b)].

Fig. 8(a) reports the evolution of the cyclic secant stiffness K_{av}^{cyc} [defined for each cycle as $K_{av}^{cyc} = (F_{\max} - F_{\min})/(U_{\max} - U_{\min})$, see Fig. 6(b)], for all MTPs during the loading program in Fig. 4. Close inspection of the figure points out mild frequency dependence during most frequency sweeps. Such effect is discussed in more detail by Kementzetzidis et al. (2021, 2023), but is not further analyzed herein. In Fig. 8(a), the range of measured K_{av}^{cyc} for all MTPs is graphically presented via diamond-headed arrows. It is evident that ranges of K_{av}^{cyc} measured between the initial and final application of a particular sweep (identical forcing) is significantly reduced for all the three presented cases; compare the black diamond-headed arrows [Fig. 8(a)], which depict the range of K_{av}^{cyc} measured during the first and the last application of the parcel with forcing $F = 5 + 2.5 \times \sin(2\pi f t)$, $f \sim 0.1$–4 Hz. Similar findings may be inferred from Fig. 8(b) for the cyclic parcels of lower frequency (0.1 Hz) and larger amplitude. Overall, swift reduction in K_{av}^{cyc} is visible in the early stage of parcels a and b, arguably due to the gradual enlargement of the pile–soil gap as increasing load levels were experienced by the piles for the first time (Kementzetzidis

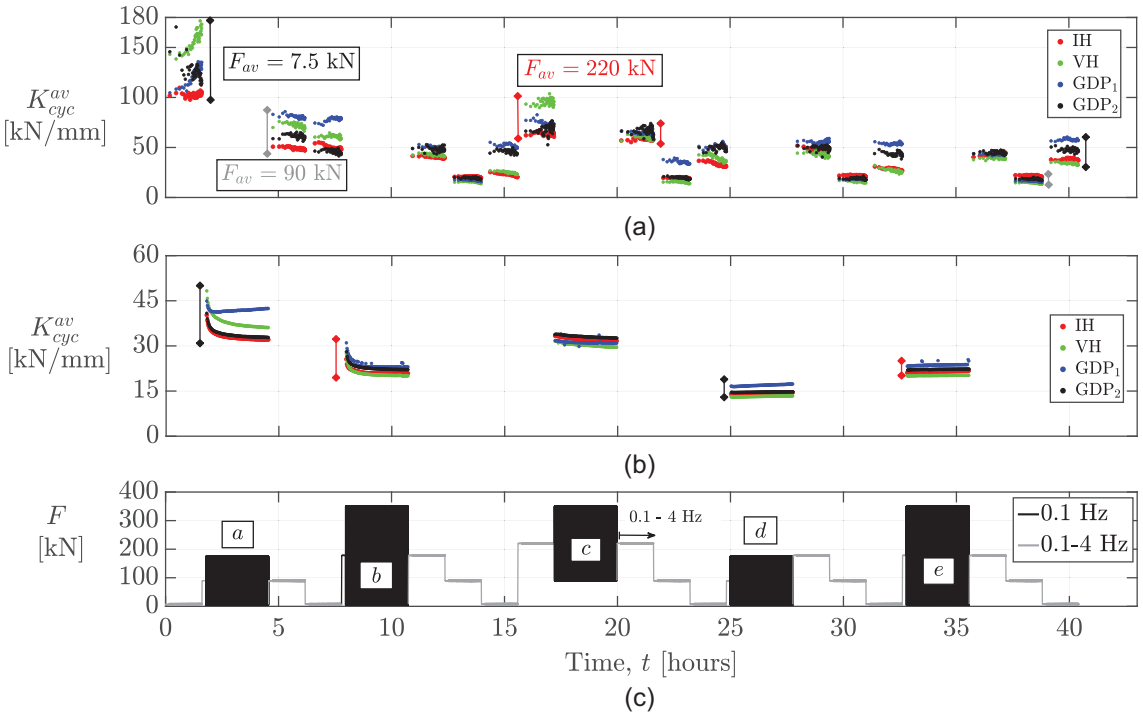

Fig. 8. (Color) Average cyclic stiffness K_{av}^{cyc} versus time t for all MPTs: (a) dynamic frequency sweeping; (b) cyclic loading of larger amplitude; and (c) applied loading program. Diamond-headed arrows in (a and b) indicate the range of measured K_{av}^{cyc} for all the MTPs during the first and last application of a particular load parcel.

et al. 2023), i.e., from 0 to 175 kN and from 175 to 350 kN for parcels *a* and *b*, respectively. Conversely, all pile responses to parcels *d* and *e* featured a modest increase in K_{av}^{cyc}, likely associated with fabric changes in the soil, including cyclic sand densification (Cuéllar et al. 2009; Liu et al. 2021; Kementzetzidis et al. 2023). Both GDP-driven piles responded to cyclic loading with (on average) the largest stiffness K_{av}^{cyc} among the four MTPs; at the same time, and in a similar fashion as for the frequency sweeps, the experimental K_{av}^{cyc} trends in Fig. 8(b) appear to converge toward very similar values for all MTPs. Such convergence of the observed pile response indicates that the loading program gradually tends to homogenize certain features of cyclic pile behavior, which are initially different due to preinstallation soil conditions (Fig. 1) and induced installation effects.

The remainder of this study exclusively focuses on the response of the MTPs to the five cyclic parcels (from *a* to *e*), which showed negligible impact of the interleaved frequency sweeps; see Fig. 5 and Kementzetzidis et al. (2023). In an attempt to distinguish possible installation effects (by accounting for the site inhomogeneity and pile–soil gapping effects), the field data shown in Figs. 5, 6, and 8(b) are interpreted in "Comparative Analysis of Pile Installation Effects" through one-dimensional (1D) pile–soil analyses based on the recent *p*–*y* model proposed by Kementzetzidis et al. (2022) (see "Modeling of Cyclic Soil Reactions").

Complementary Field Tests

To complement the experimental evidence provided by the pile installation and loading tests, additional pile impact tests were performed (Tsetas et al. 2020). Pile impact tests are well established in structural vibration testing (Brandt 2011), and have been applied to the dynamic characterization of pile–soil systems (Prendergast and Gavin 2016). During the GDP campaign at the Maasvlakte II site, similar impact experiments were conducted to identify the frequency response properties of each MTP–soil system in its pre- and postloading states (i.e., always after the pile-driving phase). The tests were performed using an instrumented hammer to hit all piles at a point located 1.5 m above the ground surface (Tsetas et al. 2020). The resulting dynamic responses were recorded for each pile by two triaxial microelectromechanical systems (MEMS) accelerometers, symmetrically positioned with respect to the location of the impact point and set to sample at 16 kHz. Finally, the recorded signals were processed to obtain experimental frequency response functions (FRFs). However, the preloading impact tests on the IH and GDP$_1$ piles returned corrupted signals due to the defective installation of some accelerometers; therefore, such data were excluded from relevant analyses.

Based on the processing of the recorded signals, Fig. 9 shows, for instance, significant differences in amplitude between the preloading FRFs obtained for the VH and GDP$_1$ piles; such differences turned out to be attenuated by the cyclic loading process, as is testified by the much closer postloading values of the FRF amplitudes and peak frequencies. In this respect, the most notable feature is the response peak at a frequency lower than 40 Hz, which is similarly observed for all piles.

Overall, the impact test results in Fig. 9 indicate a sort of homogenizing effect of prolonged cyclic loading with respect to the combined influence of pile-driving method and the soil profile features—at least for what concerns the postcyclic dynamic response to small-amplitude perturbations (and in good agreement with the stiffness data in Fig. 8).

Modeling of Cyclic Soil Reactions

This section summarizes the salient features of the cyclic *p*–*y* model used in "Comparative Analysis of Pile Installation Effects" to

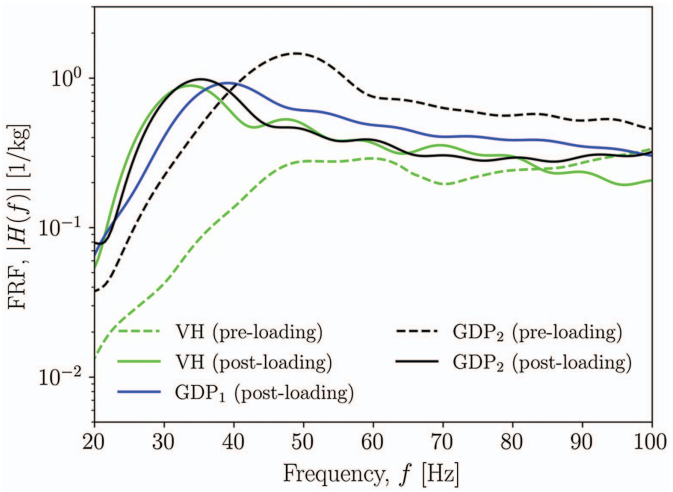

Fig. 9. (Color) Experimental frequency response functions identified for the MTP–soil systems in their pre- and postloading states.

simulate the GDP field tests. Elastoplastic modeling of drained soil reactions in water-saturated sand was carried out by combining in series a linear elastic spring and a nonlinear hysteretic element, i.e., the lateral soil displacement (y) at the interface with the pile is interpreted as the sum of two distinct components, reversible/elastic (y_e) and irreversible/plastic (y_p). The resulting cyclic soil reaction model is embedded in a comprehensive 1D rheological model for detailed modeling of gapping effects in unsaturated sand.

Elastic Component

The mentioned linear elastic component is fully characterized by the corresponding value of the stiffness K_e. In agreement with recent studies (Wan et al. 2021; Delavinia 2022), K_e was set to be directly proportional to the in situ profile of soil's small-strain shear modulus G_0 (inferred from Fig. 1)

$$K_e = 7G_0 \tag{1}$$

The influence of installation effects and cyclic loading on K_e is disregarded herein and will require further dedicated studies.

Plastic Component with Cyclic Ratcheting Control

The following ingredients of Kementzetzidis et al.'s (2022) model enable accurate simulation of (drained) pile–soil interaction in either dry or water-saturated sand, i.e., with no relevant gapping effects.

Monotonic Backbone

Under monotonic loading, the plastic component of the 1D model exactly replicates the empirical relationship by Suryasentana and Lehane (2016) between soil reaction (p) and the irreversible/plastic displacement, y_p

$$p = p_u[1 - e^{-\alpha(y_p/D)^m}] \tag{2}$$

where p_u = ultimate soil reaction force (per unit length); D = pile diameter; and α and m = dimensionless model parameters.

Extension to Cyclic Loading

The irreversible response to unloading–reloading cycles (hysteretic behavior) is reproduced via a standard kinematic hardening mechanism, resulting in the following form of the plastic modulus, K_p:

$$K_p = \frac{\alpha \cdot m}{D} \cdot |\bar{p}_u - p| \cdot \left| \frac{1}{\alpha} \ln\left(\frac{\bar{p}_u - p}{\bar{p}_u - p_0}\right) \right|^{(m-1)/m} \tag{3}$$

in which $\bar{p}_u = p_u \cdot \mathrm{sgn}(dp)$, with $\mathrm{d}p$ denoting the soil reaction increment within the current calculation step; and p_0 = projection center that takes the current p value whenever a soil reaction reversal occurs [i.e., whenever $\mathrm{sgn}(dp)$ changes]. Eq. (3) produces a mechanical response that, under monotonic loading, reduces exactly to that established by Eq. (2).

Ratcheting Control Mechanism

Excessive ratcheting in the elastoplastic p–y response under (asymmetric) cyclic loading is prevented by introducing a memory-enhancing mechanism following previous constitutive modeling studies (Corti et al. 2016; Liu et al. 2019). To this end, the model is endowed with an additional memory locus, whose size and location evolve depending on the cyclic loading history. The main role of the memory locus is to introduce an additional metric associated with the distance b_M between the current soil reaction and its projection onto the memory locus along the loading direction. The b_M is exploited to enhance the definition of the plastic modulus in Eq. (3) as follows:

$$K_{p,M} = K_p \cdot \exp \mu_0 \left(\frac{b_M}{b_{\mathrm{ref}}}\right)^2 \tag{4}$$

where μ_0 = scalar ratcheting control parameter; and $b_{\mathrm{ref}} = 2p_u$ is introduced for normalization purposes. Eq. (4) returns either $K_{p,M} = K_p$ when $b_M = 0$ (virgin loading conditions, i.e., when the soil reaction point lies on the memory locus) or $K_{p,M} > K_p$ when $b_M > 0$ due to an expansion of the memory locus induced by the previous loading history. In the latter case, the evolution of the tangent stiffness, and therefore the cyclic accumulation of lateral deflection, is controlled by the value of μ_0.

Recommendations for Parameter Calibration

The response resulting from the previous constitutive equations depends on the calibration of four parameters, namely p_u, α, m, and μ_0. Although the ratcheting parameter μ_0 may be identified by trial and error against the results of cyclic pile loading tests or advanced three-dimensional (3D) finite-element (FE) studies (Liu et al. 2021), p_u, α, and m may be set through the following cone penetration test (CPT)–based relationships inspired by the work of Suryasentana and Lehane (2016):

$$\begin{aligned} p_u &= C_{pu}\sigma'_{v0}D\left(\frac{q_c}{\sigma'_{v0}}\right)^{0.67}\left(\frac{z}{D}\right)^{0.75} \le q_c D \\ \alpha &= 8.9\left(\frac{z}{D}\right)^{-1.25}\left(\frac{\sigma_{v0} - u_g}{\sigma'_{v0}}\right)^{0.5} \\ m &= 1 \end{aligned} \tag{5}$$

where $C_{pu} = 2.4$ is the value recommended by Suryasentana and Lehane (2016); σ_{v0} and σ'_{v0} are the in situ total and effective vertical stresses at a depth z below the ground surface; and u_g = hydrostatic pore water pressure at $z = 0$. The preceding calibration procedure was numerically verified against a range of diameters (0.5–5 m), shapes (circular and square), and flexural rigidities (EI) for piles in loose to dense (in)homogeneous sand deposits (no installation effects) with variable water table depth (Suryasentana and Lehane 2014, 2016). Compliance with usual bounding surface modeling principles requires $m < 1$, which can be closely approximated by setting, e.g., $m = 0.9999$. The performance of the model under

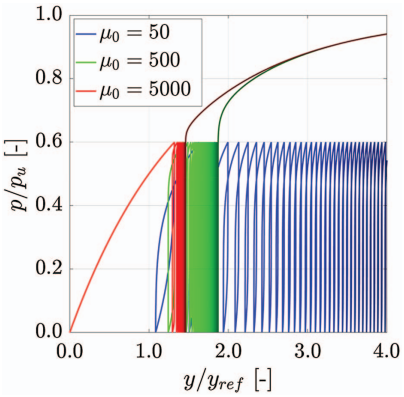

Fig. 10. (Color) Cyclic p–y soil reactions (no gapping) under $N = 100$ cycles of one-way loading ($\mu_0 = 50$, 500, 5,000). Other model parameters calibrated based on Eq. (5) for a circular pile (diameter: $D = 0.762$ m) and a soil location characterized by: $z = 4$ m (soil depth), $q_c = 17$ MPa (cone resistance), and $\gamma_{dry} = 16$ kN/m^3 (dry unit weight).

one-way cyclic loading is exemplified in Fig. 10 for different μ_0 values.

Simulation of Cyclic Pile–Soil Gapping

In the presence of cohesive soil behavior, an accurate p–y formulation should be able to reproduce pile–soil gapping, usually resulting in S-shaped lateral soil reaction curves of the kind shown in Fig. 11. Importantly, gapping effects under cyclic loading are inherently displacement dependent, as are the evolution of the gap depth and the alternation of contact–no contact stages between the pile and the soil. More details about the mechanics of pile–soil gapping are provided, e.g., by Matlock et al. (1978), Suzuki and Nakai (1985), Boulanger et al. (1999), and Kementzetzidis et al. (2023). As previously mentioned, gapping effects were clearly exhibited by all pile loading data recorded at the Maasvlakte II site (Fig. 6) due to the unsaturated soil above the water table.

Following Kementzetzidis et al. (2022), lateral soil reactions in the upper unsaturated sand have been modeled by combining the above memory-enhanced p–y model—the memory spring—with

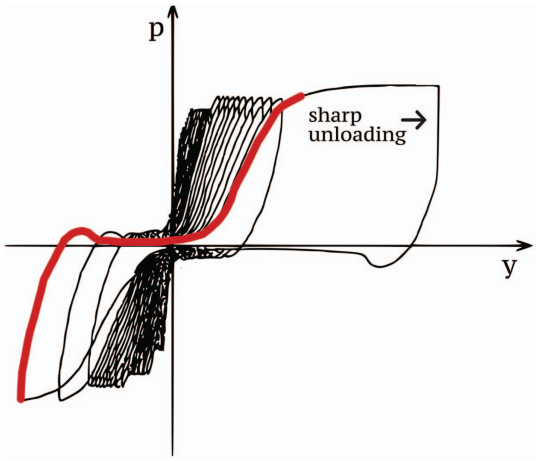

Fig. 11. (Color) Cyclic p–y curves for cohesive soils. The thick line highlights the mentioned S-shape of the last p–y response cycle (adapted from Randolph and Gourvenec 2011; Bea et al. 1979).

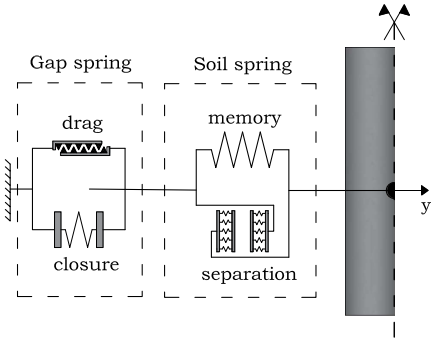

Fig. 12. 1D modeling scheme for the simulation of cyclic hysteresis with ratcheting control and pile–soil gapping, left side of the pile only; a similar scheme is also applied to the right side (adapted from Kementzetzidis et al. 2022).

additional rheological elements, namely, the so-called separation, closure, and drag springs. Fig. 12 illustrates (half of) the resulting pile–soil interaction scheme. The inherent asymmetry of the gapping mechanism requires the use of two distinct interaction elements on both sides of the pile.

Separation Spring

The separation spring enables the simulation of the sharp unloading branch that originates at the onset of pile–soil separation (Fig. 11). Due to the lack of dedicated data for calibration, the separation spring is deactivated in the global pile–soil interaction scheme, and for brevity not further described herein; more details are available in Kementzetzidis et al. (2022). For the pile loading cases considered in the following, the stiffening that is necessary to simulate the mentioned stiff unloading response is directly provided by the parallel memory mechanism (Fig. 12).

Closure Spring

The inclusion of the so-called closure spring is required to simulate the peculiar shape (resembling a rotated S) of the p–y response cycles in the presence of cohesive soil behavior (Boulanger et al. 1999) (Fig. 11). To reproduce mathematically such a shape, the following function—similar to Eq. (2)—is adopted to relate, in finite terms, the reaction component in the closure spring (p_c) to the corresponding displacement (y_g, i.e., the displacement of the overall gap spring in Fig. 12):

$$p_c = p_{c,\max}\left(e^{-\alpha_c|(y_g - y_{g,0})/y_{\max}|^{m_c}}\right) \tag{6}$$

where m_c and α_c = dimensionless shape parameters; while $y_{g,0}$ assumes the current value of y_g every time the pile re-enters the gap from a new $y_{\max}$.

The formulation of the closure spring was chosen to represent the shape of pile–soil interactions when the pile moves inside the gap and ensures that upon unloading from $p_c = p_{c,\max}$, the closure spring reaches a nil asymptote ($p_c = 0$) as fast as enabled by the selected pair of m_c-α_c values (shape parameters), so as to reproduce the desired S-shape of the p–y response. More information on the impact of such parameters on the gapping soil reactions is available in Kementzetzidis et al. (2022). Values in the order of $m_c = 0.6$ and $\alpha_c = 20$ have been found to provide a reasonable gap-closing response for a sharp pile–soil separation, and are henceforth considered as a first-guess pair of calibrated parameters.

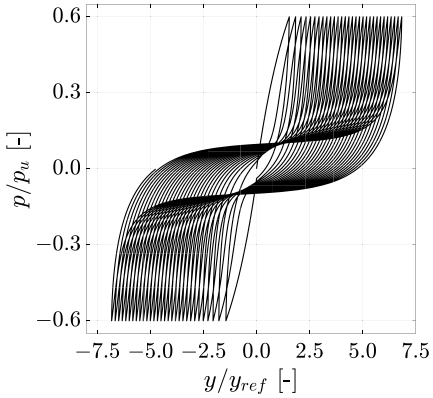

Fig. 13. Cyclic p–y soil reactions (with gapping) under symmetric/two-way loading. Model parameters calibrated based on Eq. (5) for a circular pile (diameter: $D = 0.762$ m) and a soil location characterized by $z = 4$ m (soil depth), $q_c = 17$ MPa (cone resistance), $\gamma_{dry} = 16$ kN/m^3 (dry unit weight). Additionally: $\mu_0 = 20$, $\alpha_c = 5$, $m_c = 0.6$, and $C_d = 0.1$.

Combined Memory and Drag Springs

A gapping p–y model should also reproduce the frictional resistance offered by the side soil wall when normal contact is lost on either one or both sides of the pile. Frictional drag (side pile–soil friction, introduced via the drag spring) resists pile motion regardless of the pile location and displacement direction within the gap area. In the model of Kementzetzidis et al. (2022), the drag soil reaction component, p_d, is described as follows:

$$p_d = p_{u,d}(1 - e^{-\alpha[(|y_g - y_g^r|)/D]^m}) \tag{7}$$

where $p_{u,d} = C_d p_u$, with C_d being a scalar parameter that can be tuned between 0 and 1 to modulate the relative contribution of the drag reaction to the total lateral soil resistance. Therefore, to preserve the total ultimate soil resistance, the quota associated with the memory spring is reduced to $p_{u,m} = (1 - C_d)p_u$. Additionally, $y_g^r = y_g$ is updated at every sign reversal of $\dot{y}_g$ (at the beginning of the analysis, the initialization $y_g^r = y_g = 0$ is set). Eqs. (2) and (7) are identical for monotonic loading conditions, which allows the use of the CPT calibration procedure by Suryasentana and Lehane (2016) also for the complete gapping p–y model. The response of the gapping and ratcheting enhanced cyclic p–y model to two-way loading is presented in Fig. 13.

1D Pile–Soil Model Setup

To simulate the reference pile loading tests, 1D FE models were set up for the four MTPs using the OpenSees simulation platform (McKenna 2011), in which the complete p–y model described previously was implemented. To this end, the four identical piles were idealized as Timoshenko beams, with their embedded length (8 m below ground surface) set in contact with a sequence of gapping (upper 4 m, in the unsaturated soil) and nongapping (lower 4 m) spring elements with a vertical spacing of 8 cm (Fig. 14). The calibration of all soil reaction parameters is discussed in the following section along with the simulation of the four MTP loading tests.

Comparative Analysis of Pile Installation Effects

In this section, the response of all the MTPs to the cyclic loading program in Fig. 4 is quantitatively analyzed using the elastoplastic p–y model presented in "Modeling of Cyclic Soil Reactions."

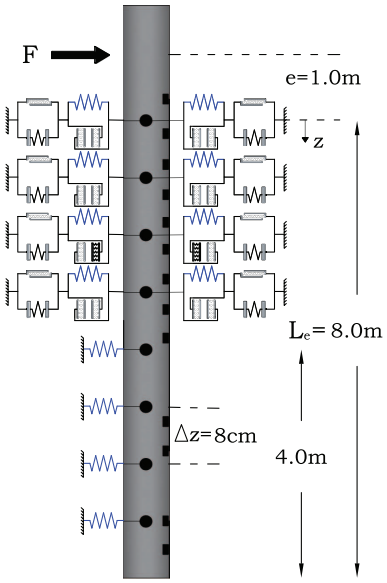

Fig. 14. (Color) Reference 1D pile model subjected to lateral cyclic loading. The ground water table depth ($z = 4$ m) marks the transition between unsaturated and saturated soil. The black rectangular symbols indicate the locations of the fiber bragg grating (FBG) axial strain sensors.

Given the different soil profiles at the four pile locations (Fig. 1), such analysis aims to filter out differences in lateral response features that are mainly related to preinstallation soil conditions.

General Considerations

For each loading test, the first loading branch in Parcel a (highlighted in Fig. 6)—from 0 to $F = 175$ kN—may be regarded as a postinstallation stage of monotonic loading. The measured load–displacement curves are reported in Fig. 15 for all MTPs, along with their numerically simulated counterparts (dashed lines). It is possible to observe that, in absolute terms, the VH pile was the stiffest of all piles (although installed in the loosest/softest sand profile, compare to Fig. 1), followed by the GDP-driven piles ($GDP_{1,2}$) and, finally, the IH pile (impact-hammered). Quite surprisingly, GDP_1 and GDP_2 exhibited almost identical monotonic responses, despite the non-negligible differences in terms of preinstallation q_c profile at the respective locations.

The cyclic pile deflection trends presented in Figs. 5 and 6 seem to contradict the conclusions drawn on the sole basis of the monotonic response curves. Regarding the impact of the five cyclic parcels in Fig. 4 (5,000 cycles in total), it may be stated that:

- While the VH pile was monotonically the stiffest (which is seemingly in contradiction with the corresponding q_c profile), it accumulated the second largest cyclic deflection by the end of the cyclic loading sequence;
- Cyclic deflection accumulation was lowest for the two GDP piles (Figs. 5 and 6), in a fashion that is consistent with the respective preinstallation soil profiles (i.e., GDP_2 displaced less than GDP_1 with $q_c^{GDP_1}$ being on average lower than $q_c^{GDP_2}$);
- The IH pile experienced the largest lateral deflection, both monotonically (first segment of Parcel a) and cyclically (over the whole loading program).

In more detail, the VH pile accumulated during Parcel a the lowest lateral deflection at the ground surface, while it displaced more than both GDP-driven piles by the end of Parcel e: this outcome is arguably the result of a complex interaction between initial soil

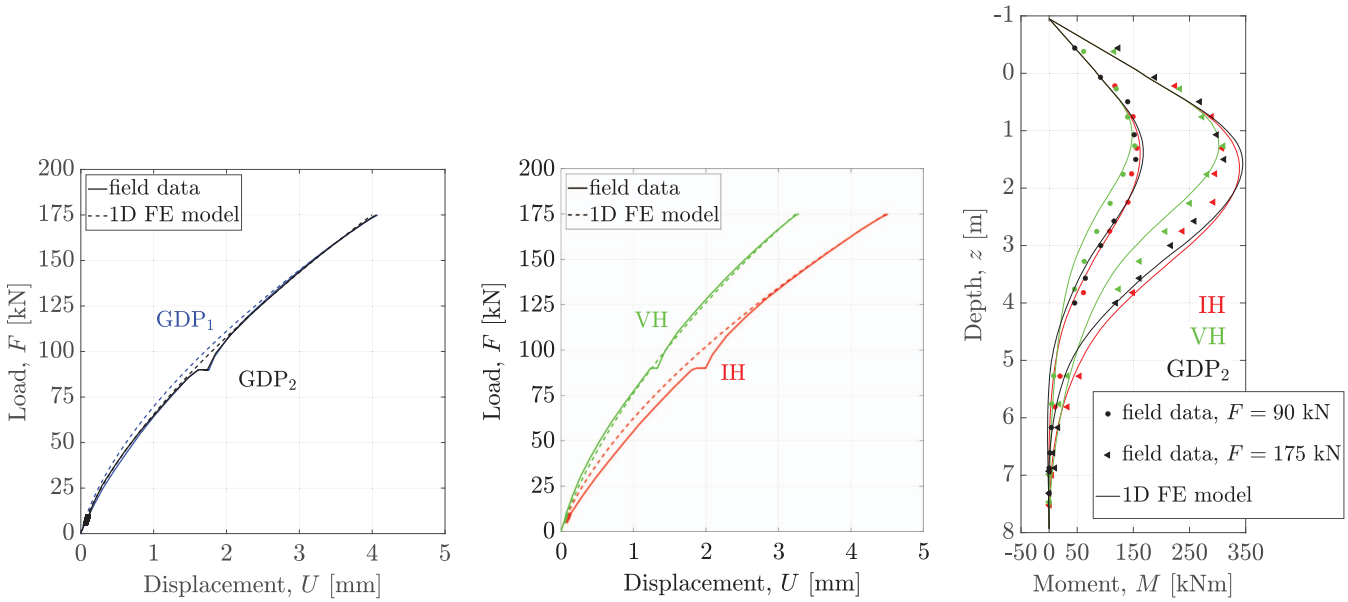

Fig. 15. (Color) Measured and calculated force–displacement responses and selected bending moment profiles [associated with $F = 90$ kN and $F = 175$ kN in Parcel a, monotonic branch ($N = 1$); see Figs. 4 and 6]. GDP_1's bending moment profiles were deemed unreliable (sensor malfunctioning) and therefore omitted.

conditions and pile installation effects, where the latter seem to be working differently depending on the preinstallation relative density profile; see also the previous studies of Staubach et al. (2020), Bienen et al. (2021), and Fan et al. (2021a, b). Because the VH pile was installed in substantially looser sand than the other MTPs, it is preferred to focus in what follows on the comparison between GDP-driven and impact-hammered (IH) piles, which were all installed in medium-dense to dense sand. Such an option was ultimately suggested by the modeling outcomes in "Quantitative 1D FE Studies."

Quantitative 1D FE Studies

The measured differences in the lateral response of the otherwise identical MTPs may be attributed to differences in the installation procedures and the foundation soil. Relevant p–y model parameters were calibrated, both for the saturated and the unsaturated soil layers, by first identifying those governing the monotonic lateral response (i.e., K_e, p_u, α, and m). The elastic component of the memory springs was calibrated as $K_e = 7G_0$, as obtained from the shear velocity profiles in Fig. 1. For p_u, α, and m, a first calibration attempt was made by following the CPT-based procedure proposed by Suryasentana and Lehane (2016) and reported in Eq. (5). The resulting comparison between field data and first-trial simulations was rather unsatisfactory, probably due to the applied monotonic load being relatively low compared to the reference load range considered by Suryasentana and Lehane (2016), who examined monotonic pile responses up to the reference capacity $U = 0.2D$. The same calibration strategy described by Kementzetzidis et al. (2022) was applied to the four MTPs to improve the agreement between measured and simulated monotonic load–displacement curves. It was first found to be beneficial to reduce the value of m, from 1 to 0.5 for all piles; then new C_{pu} values were recalibrated as reported in Table 3 [compare to Eq. (5)], with direct impact on the local ultimate resistance of each p–y element. The retuned C_{pu} values produced the satisfactory matches shown in Fig. 15 for all piles, both in terms of load–displacement curves and bending moment profiles at two distinct load levels (90 and 175 kN). The explicit q_c dependence of p_u in (the first line of) Eq. (5) accounts for the inhomogeneity of soil properties down the pile, so it may be argued that C_{pu} is directly representative of pile installation effects—particularly for piles that are geometrically identical. In this respect, Table 3 indicates that:

- In spite of quite different average cone resistance values ($q_{c,av}$) down the pile, almost identical C_{pu} values were identified for the GDP-driven piles, which suggests a strong correlation of C_{pu} with the pile-driving technology.
- The response of piles installed in medium-dense to dense sands was reproduced by similar C_{pu} values: compare $GDP_{1,2}$ and IH to VH. GDP-driven piles were found to be represented by C_{pu} values that are approximately 13% larger than for the impact-hammered pile. This outcome establishes the same relationship between the respective soil resistance values (p_u), and would theoretically extend to the (very) ultimate pile capacity defined as $F_{ult} = \int_0^{L_e} p_u dz$. Conversely, a slightly different capacity increment (+ 15%) is estimated in "Predicted Installation Effects in a Fictitious Sand Deposit" for GDP and IH piles in the same soil profile by adopting a conventional definition of lateral capacity (i.e., the load inducing a lateral pile deflection $U = 0.1D$ at the ground surface).
- The response of the VH pile installed in loose sand was reproduced using C_{pu} values approximately 85% larger than those

Table 3. Values of C_{pu} and C_{μ_0} [from Eqs. (5) and (8)] set to fit the measured monotonic and cyclic lateral pile responses at the Maasvlakte II site, Figs. 15 and 16

Parameter	GDP_1	GDP_2	IH	VH
$q_{c,av}$ (MPa)	12.4	21.3	14.9	6.4
C_{pu}	0.417	0.411	0.365	0.674
$C_{\mu 0}$	310	181	282	165

Note: $q_{c,av}$ = average q_c along the embedded length of each pile, compare to Fig. 1. The rightmost column highlights that VH data are considered less meaningful for comparison purposes (see discussion in "Comparative Analysis of Pile Installation Effects").

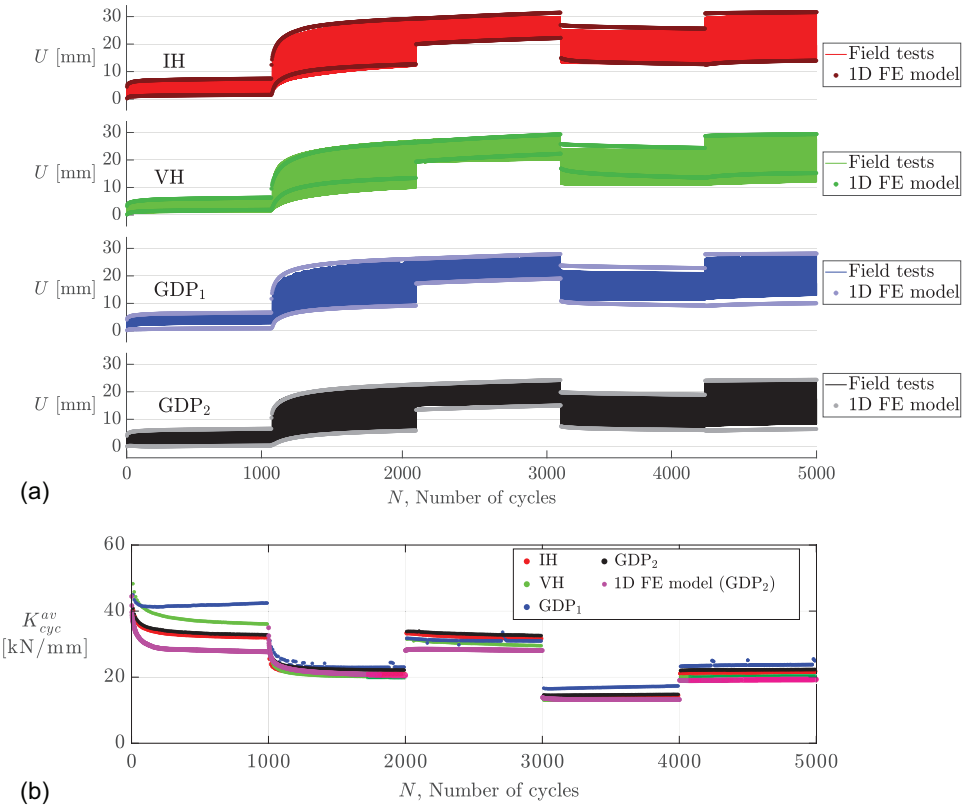

Fig. 16. (Color) (a) Cyclic pile deflection trends (deflection measured at the soil surface); and (b) evolution of K_{cyc}^{av} [defined in Fig. 6(b)] induced by the cyclic load parcels ($a-e$) in Fig. 4 on the four MTPs. In (a), the p–y simulation results (dotted lines indicate cyclic deflection bounds) are compared to measured data (solid lines). In (b), the K_{cyc}^{av} trend simulated for the GDP_2 pile is shown in magenta.

identified for the impact-driven pile. Special caution should be devoted when linking this output to the quantitative interpretation of installation effects for the VH pile, which was installed in a significantly different (looser) soil profile in comparison to the others; see subsequent discussion.

The same philosophy for analyzing pile installation effects was also applied to the measured cyclic responses. To this end, additional p–y model parameters had to be calibrated, namely, μ_0 (ratcheting control parameter), C_d (frictional drag resistance parameter), and the shape parameters α_c and m_c governing the behavior of the closure spring (Fig. 12). Following Kementzetzidis et al. (2022), the values of $m_c = 0.5$, $\alpha_c = -\ln(0.15)/(0.55)^{m_c}$, and $C_d = 0.0$ were first set (equal for all piles). In a further attempt to reduce the calibration effort, the frictional drag mechanism ("Simulation of Cyclic Pile–Soil Gapping") was inhibited by setting $C_d = 0.0$. In fact, Kementzetzidis et al. (2022) showed the modest impact of frictional drag for piles subjected to one-way cycling. Finally, the following CPT-based relationship was assumed for the calibration of μ_0:

$$\mu_0 = C_{\mu_0} \cdot \left(\frac{q_c}{\sigma'_{v0}}\right)^{0.1} \left(\frac{\sigma'_{v0}}{\sigma'_{v,\text{ref}}}\right)^{0.75} \tag{8}$$

where C_{μ_0} = scalar dimensionless parameter; and $\sigma'_{v,\text{ref}} = \gamma' z$ kPa (for $z = 1$ m, and γ' the effective unit weight of soil) serves as a reference vertical effective stress. According to Eq. (8), μ_0 is assumed to depend on both q_c and z. The adopted z dependence is similar to that considered for p_u in Eq. (5), while the type of q_c dependence was identified through trial and error to enable the simulation of all MTP responses using only C_{μ_0} as a location- or installation-specific parameter. Because the same soil unit weight and pile geometry apply to all MTPs, it was not necessary to introduce additional factors in Eq. (8) for the purposes of this study. The C_{μ_0} values in Table 3 were identified for all piles to obtain a good match between experimental and simulated cyclic deflection trends at the ground surface—respectively the solid and dotted lines in Fig. 16(a). Apparently, the numerical model reproduces very well the field measurements associated with all MTPs, including the peculiar displacement relaxation observed during the fourth cyclic load parcel (d). See also Liu et al. (2022) about the performance of memory-enhanced bounding surface models under multiamplitude cyclic loading histories.

The same evolution trends of the average cyclic stiffness (K_{av}^{cyc}) discussed in "Cyclic Lateral Loading Tests" are also compared in Fig. 16(b); for clearer illustration, only those obtained for the GDP_2 pile (in magenta). Apart from the generally good agreement between measured and simulated trends, a closer inspection of relevant internal variables in the p–y model confirmed some of the claims made by Kementzetzidis et al. (2023) on a purely experimental basis: (1) the drop in K_{av}^{cyc} during parcels $a-b$ relates to the main gap-opening events; (2) when an approximately steady size of the gap is maintained (here during parcels $d-e$), the model captures the gradual increases in cyclic stiffness through the expansion of the memory loci along the different p–y springs [increase of b_M in Eq. (4)].

The complete response of the main test piles to the whole cyclic loading program is compared to the corresponding field data regarding the load–displacement response in Figs. 17 and 18, and bending moment profiles at selected loading instants (referred to as

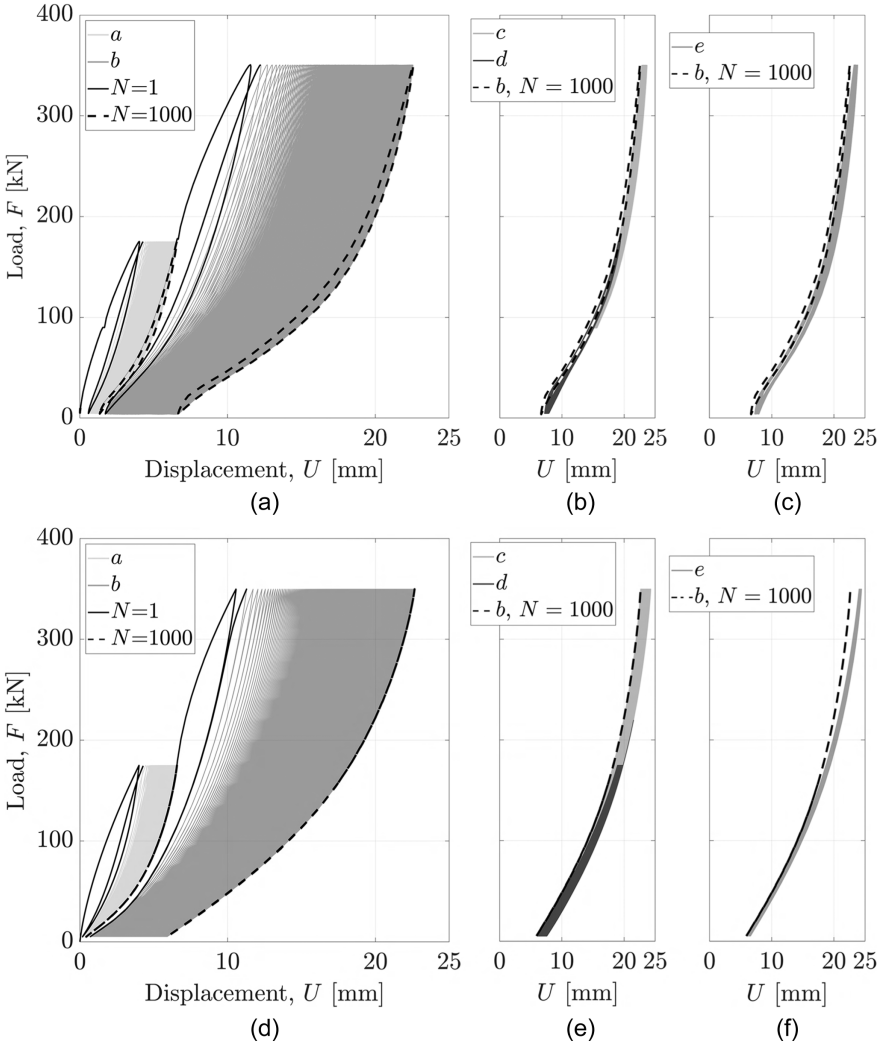

Fig. 17. (a–c) Measured and (d–f) calculated force-displacement responses of GDP2 to: (a, d) Parcels *a* and *b*; (b, e) Parcels *c* and *d*; and (c, g) Parcel *e* in Fig. 4.

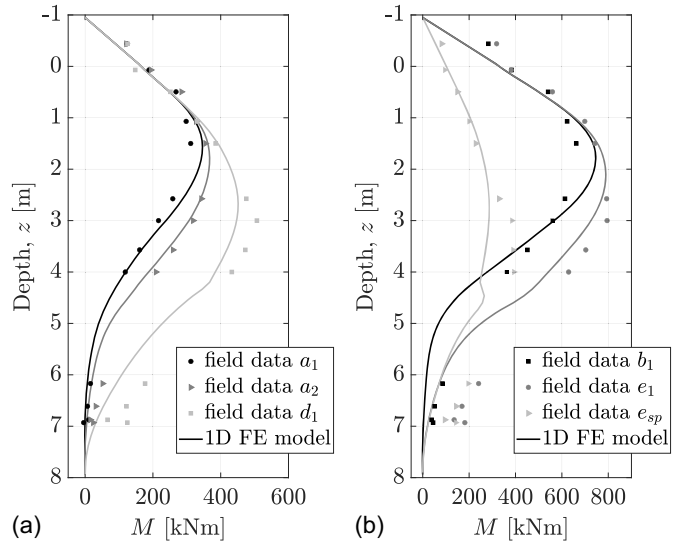

Fig. 18. GDP_2: Measured (markers) and calculated (solid lines) bending moment profiles; the times at which bending moment profiles were measured or calculated along the loading program (e.g., α_1, α_2) are indicated as in Fig. 4.

a_1, a_2, b_1, d_1, e_1, and e_{sp} in Figs. 4 and 18); for brevity, only for the GDP_2 pile. The results obtained testify once again to the suitability of the adopted 1D modeling framework, especially when considering the complexity introduced by multiamplitude cycling and shallow unsaturated soil conditions.

Overall, the results presented in this section demonstrate the merits of the 1D FE model, as well as the consistency of a parameter calibration strategy that worked properly for all MTPs. It is thus possible to draw some final considerations suggested by the calibrated $C_{\mu 0}$ values in Table 3 (the value calibrated for the VH pile is mostly regarded as an outlier, given the significantly lower density of the soil at that location):

- $C_{\mu 0}$ appears to be (negatively) correlated with the average cone resistance, $q_{c,av}$, rather than with the pile-driving method [Fig. 19(a)]. This observation is further supported by the comparison of the MTP force–displacement responses replotted in Fig. 19(b) after normalizing the lateral deflection by its value U_{mon} at the end of the initial monotonic branch (i.e., prior to Parcel *a* cycling). Apparently, such a normalization highlights the mentioned correlation between cyclic ratcheting response and soil profile features (compare to Fig. 1).
- At variance with what observed for postinstallation monotonic responses (Fig. 15), prolonged lateral cycling seems to gradually erase or homogenize certain installation effects.

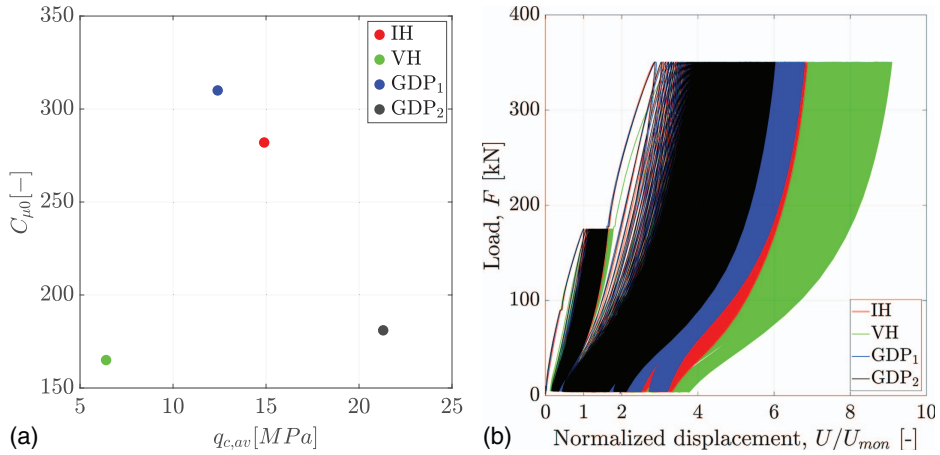

Fig. 19. (Color) (a) Values of C_{μ_0} versus $q_{c,av}$ from Eq. (8) set to fit the measured monotonic and cyclic lateral pile responses at the Maasvlakte II site. The observed trend further supports that the VH data are less suitable for comparison purposes (see discussion in "Comparative Analysis of Pile Installation Effects"); and (b) force versus normalized displacement response of the MTPs under the cyclic loading program in Fig. 4. Normalization is by the value U_{mon} of lateral pile deflection at the end of the initial monotonic branch (i.e., prior to Parcel a cycling).

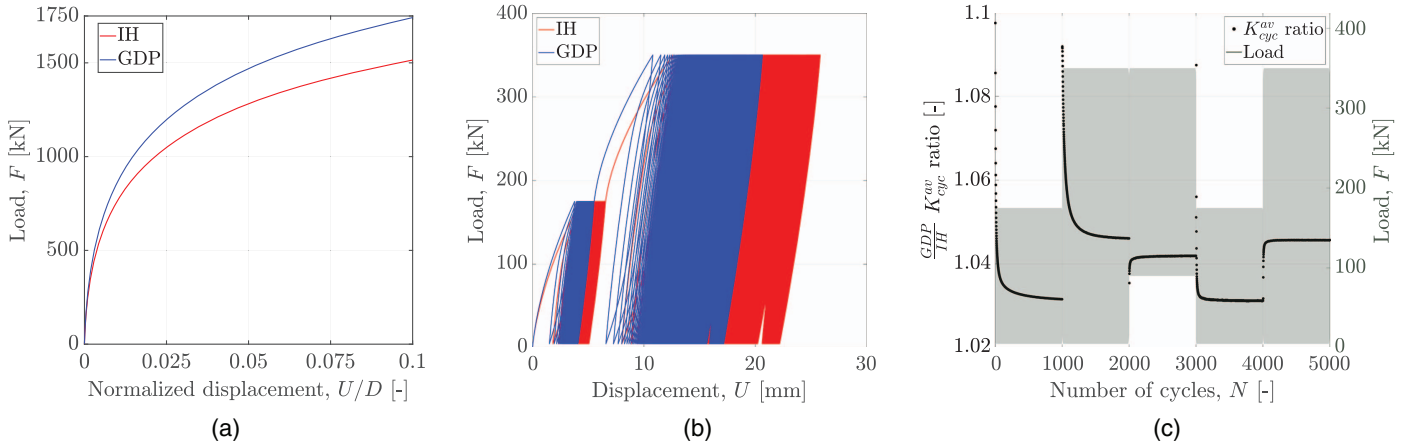

Fig. 20. (Color) Simulated force–displacement response of impact- and GDP-driven piles at a fictitious saturated sandy site. Response to (a) monotonic loading (up to conventional capacity); (b) the cyclic loading program in Fig. 4; and (c) simulated GDP-to-IH ratio of lateral cyclic stiffness versus number of loading cycles.

Predicted Installation Effects in a Fictitious Sand Deposit

The analysis of both measured and simulated pile responses at the Maasvlakte II site in "Comparative Analysis of Pile Installation Effects" highlights marked pile installation effects. Importantly, the trends of cyclic pile stiffness obtained from measured data exhibit a sort of homogenizing tendency under prolonged cyclic loading [Figs. 9 and 16(b)]. To reinforce the model-based interpretation of such installation effects, the same 1D FE model was used to simulate the lateral behavior of two piles (identically sized as the MTPs; Table 1) installed through impact hammering and GDP in a fictitious fully saturated sandy site—therefore, with no gapping effects under lateral loading. The fictitious site was characterized by averaging the q_c and V_s profiles associated with the IH and GDP_1 pile locations (Fig. 1); then 1D model parameters were calibrated for the two piles by setting $K_e = 7G_0$, while α, m, and $\mu 0$ were obtained through correlation to the fictitious V_s and q_c profiles; $C_{\mu 0} = 296$ was determined as a representative value for the assumed average q_c profile [Fig. 19(a)]. In agreement with the analysis in "Quantitative 1D FE Studies," all installation effects were lumped into the calibrated p_u profiles, which ware determined using Eq. (5) with the C_{pu} values reported in Table 3 (an average $C_{pu} = 0.414$ was selected for the GDP method). Both piles were monotonically loaded up to their conventional lateral capacity ($U = 0.1D = 0.0762$ m); then separate cyclic simulations were performed considering cyclic loading program in Fig. 4.

The simulated monotonic behavior of impact-hammered and GDP-installed piles is shown in Fig. 20(a). As expected, the differences in the corresponding p_u profiles determine a stiffer response of the GDP pile, with a larger load (conventional capacity) necessary to achieve a displacement at ground surface equal to $U = 0.1D - F = 1{,}740$ kN and $F = 1{,}514$ kN for the GDP- and the impact-driven piles, respectively. The ratio between (conventional) capacities for the two piles ($1{,}740/1{,}514 \approx 1.15$) is slightly larger than the ratio between the respective values of the soil resistance parameter C_{pu} (see "Quantitative 1D FE Studies").

As for the simulated cyclic response, the two piles are predicted to accumulate significantly different lateral deflection [Fig. 20(b)]. In particular, the final deflection associated with the impact-driven pile is almost 30% larger at the ground surface, notwithstanding the use of the same ratcheting control parameter μ_0 [due to identical q_c profiles and C_{μ_0} values for the two piles; see also Eqs. (4) and (8)].

Regarding the cyclic evolution of the K_{av}^{cyc} stiffness, the 1D model predicts a similar homogenization effect of cyclic loading as suggested by the preceding field data. This statement is supported by Fig. 20(c), which displays the evolving GDP-to-IH K_{av}^{cyc} ratio. According to the 1D model, while the cyclic stiffness of the GDP pile is initially $\approx$10% larger, a tendency toward very small differences is obtained as more loading cycles are applied. After a few thousand cycles, an approximately steady difference of $\approx 3\% - 4.5\%$ results for all load parcels.

Conclusions

To compare the novel GDP driving method to more traditional approaches, four piles (MTPs) were driven in sandy soil via impact hammering (one pile), axial vibro-driving (one pile), and the GDP method (two piles). In this study, the postinstallation lateral loading test results from the GDP field campaign were analyzed and modeled in detail to assess the impact of the pile installation method.

All MTPs were subjected to the same complex cyclic loading program comprising $N = 82{,}000$ loading cycles in total, 5,000 of which featured low frequency (0.1 Hz) and relatively large amplitude, the main focus of this study. The results of the first GDP field campaign indicated that, overall, GDP-driven piles responded to cyclic loading better than the other IH- and VH-installed piles. At the same time, it was important to recognize the inevitable impact of unsaturated soil conditions (in the shallowest 4 m of the site) and geotechnical inhomogeneities, which altogether hindered a fair comparison of all measured pile responses on a pure data-analysis basis. To overcome this difficulty, pile performances were indirectly (but more fairly) compared through the parameters of an advanced cyclic p–y model calibrated for each MTP, specifically accounting for the differences in cone resistance profile at the reference pile locations. Furthermore, by using the same calibration settings obtained by fitting the pile responses observed at the Maasvlakte II site, installation effects that could be found at a marine site (i.e., with no gapping effects in water-saturated soil) were reevaluated for impact- and GDP-driven piles, based on the simulation of monotonic and cyclic lateral pile behavior at a fictitious sandy site.

The main findings regarding pile installation effects in the response to lateral loading may be summarized as follows:

postinstallation monotonic response

- Laterally loaded piles may exhibit significant installation effects during loading phases that are immediately postinstallation, especially for relatively low lateral load amplitudes; data indicate up to approximately 15% of the monotonic capacity (Fig. 15). Despite differences in initial soil profiles, the GDP-installed piles responded identically during this stage.
- Numerical simulations based on the calibrated 1D FE model described in this paper indicate that, in medium-dense to dense sand, the GDP method may result in a lateral capacity approximately 15% larger than for a pile impact hammered at an identical soil location.

postinstallation cyclic response

- Noticeable differences are present in the residual accumulated lateral deflection for piles installed via different installation methods in different soil profiles (Fig. 6). The results of 1D FE simulation suggest that such differences between installation methods would still be observed at identical installation sites ("Comparative Analysis of Pile Installation Effects").
- After normalizing the cyclic response of all MTPs by the maximum monotonic displacement attained prior to cyclic loading (in an attempt to filter our installation effects), the measured trends of cyclic deflection accumulation correlate altogether with soil profile features at the respective pile locations [compare Figs. 1 and 19(b).] This finding is further supported by the identified parameters of the adopted 1D numerical model. Particularly, the ratcheting control parameter $C_{\mu 0}$ appears to be more strongly correlated with the average cone resistance $q_{c,av}$ [Fig. 19(a)] than with the specific pile installation method.
- Initial differences in lateral pile stiffness were attributed to the joint effect of the installation method and initial soil conditions. Such differences (in the cyclic lateral pile stiffness) were both measured (field data) and simulated (1D FE model) to depend on the particular loading parcel and to gradually diminish under the application of an increasing number of loading cycles. The two GDP-driven piles exhibited, on average, the largest cyclic lateral stiffness in comparison with the other MTPs.

The preceding conclusions do not include observations regarding the pile that was axially vibrated into substantially looser sand (VH). Describing the interaction between initial sand density and pile-driving method will require additional experimental data and numerical modeling work. These and other open questions are currently being investigated in the framework of the SIMOX (GROW 2016) joint industry project.

Data Availability Statement

Some or all data, models, or code generated or used during the study are proprietary or confidential in nature and may only be provided with restrictions.

Acknowledgments

This paper is associated with the GDP project in the framework of the GROW joint research program. Funding from *Topsector Energiesubsidie van het Ministerie van Economische Zaken* under Grant No. TEHE117100 and financial/technical support from the following partners is gratefully acknowledged: Royal Boskalis Westminster N.V., CAPE Holland B.V., Deltares, Delft Offshore Turbine B.V., Delft University of Technology, ECN, Eneco Wind B.V., IHC IQIP B.V., SHL Offshore Contractors B.V., Shell Global Solutions International B.V., Sif Netherlands B.V., TNO, and Van Oord Offshore Wind Projects B.V. The important contribution to the GDP field campaign of, in alphabetical order, Rob Atkinson, Kees van Beek, Ahmed Elkadi, Sergio S. Gómez, Timo Molenkamp, Maxim L. A. Segeren, Faraz S. Tehrani, Apostolos Tsouvalas, and Peter de Vries is also warmly appreciated.

References

Achmus, M., K. A. Schmoor, V. Herwig, and B. Matlock. 2020. "Lateral bearing behaviour of vibro-and impact-driven large-diameter piles in dense sand." *Geotechnik* 43 (3): 147–159. https://doi.org/10.1002/gete.202000006.

Anusic, I., B. Lehane, G. Eiksund, and M. Liingaard. 2019. "Influence of installation method on static lateral response of displacement piles in sand." *Géotech. Lett.* 9 (3): 193–197. https://doi.org/10.1680/jgele.18.00191.

Bea, R. G., J. M. E. Audibert, and M. R. Akky. 1979. "Earthquake response of offshore platforms." *J. Struct. Div.* 105 (2): 377–400. https://doi.org/10.1061/JSDEAG.0005099.

Bienen, B., S. Fan, M. Schröder, and M. F. Randolph. 2021. "Effect of the installation process on monopile lateral response." *Proc. Inst. Civ. Eng. Geotech. Eng.* 174 (5): 530–548. https://doi.org/10.1680/jgeen.20.00219.

Boulanger, R. W., C. J. Curras, B. L. Kutter, D. W. Wilson, and A. Abghari. 1999. "Seismic soil-pile-structure interaction experiments and analyses." *J. Geotech. Geoenviron. Eng.* 125 (9): 750–759. https://doi.org/10.1061/(ASCE)1090-0241(1999)125:9(750).

Brandt, A. 2011. *Noise and vibration analysis: Signal analysis and experimental procedures*. New York: Wiley.

Byrne, B. W., et al. 2020a. "PICASO: Cyclic lateral loading of offshore wind turbine monopiles." In *Proc., 4th Int. Symp. on Frontiers in Offshore Geotechnics (ISFOG 2021), Frontiers in Offshore Geotechnics IV*, edited by Z. Westgate, 1526–1535. Leiden, Netherlands: CRC Press.

Byrne, B. W., R. A. McAdam, W. J. Beuckelaers, H. J. Burd, K. Gavin, G. T. Houlsby, D. J. P. Igoe, R. Jardine, and C. M. Martin. 2020b. "Cyclic laterally loaded medium scale field pile testing for the PISA project." In *Proc., 4th Int. Symp. on Frontiers in Offshore Geotechnics (ISFOG 2021), Frontiers in Offshore Geotechnics IV*, edited by Z. Westgate, 1323–1332. Leiden, Netherlands: CRC Press.

Corti, R., A. Diambra, D. M. Wood, D. E. Escribano, and D. F. Nash. 2016. "Memory surface hardening model for granular soils under repeated loading conditions." *J. Eng. Mech.* 142 (12): 04016102. https://doi.org/10.1061/(ASCE)EM.1943-7889.0001174.

Cuéllar, P., M. Baeßler, and W. Rücker. 2009. "Ratcheting convective cells of sand grains around offshore piles under cyclic lateral loads." *Granular Matter* 11 (6): 379. https://doi.org/10.1007/s10035-009-0153-3.

Delavinia, D. 2022. "Seismic response of monopile foundations for offshore wind turbines: From 3D to 1D modelling of soil-foundation interaction." Master's thesis, Faculty of Civil Engineering and Geosciences, Delft Univ. of Technology.

Fan, S., B. Bienen, and M. F. Randolph. 2021a. "Effects of monopile installation on subsequent lateral response in sand. I: Pile installation." *J. Geotech. Geoenviron. Eng.* 147 (5): 04021021. https://doi.org/10.1061/(ASCE)GT.1943-5606.0002467.

Fan, S., B. Bienen, and M. F. Randolph. 2021b. "Effects of monopile installation on subsequent lateral response in sand. II: Lateral loading." *J. Geotech. Geoenviron. Eng.* 147 (5): 04021022. https://doi.org/10.1061/(ASCE)GT.1943-5606.0002504.

Fredlund, D. G. 2006. "Unsaturated soil mechanics in engineering practice." *J. Geotech. Geoenviron. Eng.* 132 (3): 286–321. https://doi.org/10.1061/(ASCE)1090-0241(2006)132:3(286).

Gaertner, E., et al. 2020. *IEA wind TCP task 37: Definition of the IEA 15-megawatt offshore reference wind turbine*. Golden, CO: National Renewable Energy Lab.

GROW (Growth Through Research, Development & Demonstration in Offshore Wind). 2016. "Sustainable installation of XXL monopiles (SIMOX)." Accessed June 30, 2023. https://www.grow-offshorewind.nl/project/simox.

Heins, E., and J. Grabe. 2017. "Class-a-prediction of lateral pile deformation with respect to vibratory and impact pile driving." *Comput. Geotech.* 86 (Mar): 108–119. https://doi.org/10.1016/j.compgeo.2017.01.007.

Herwig, V., and J. Gattermann. 2015. "Vibro-project–vergleich der lateralen tragfähigkeit von vibrierten und geschlagenen stahlpfählen in sandigen böden." In Vol. 19 of *Proc., Pfahl-Symp*. Brunswick, Germany: Technical Univ. of Braunschweig.

Igwemezie, V., A. Mehmanparast, and A. Kolios. 2019. "Current trend in offshore wind energy sector and material requirements for fatigue resistance improvement in large wind turbine support structures—A review." *Renewable Sustainable Energy Rev.* 101 (May): 181–196. https://doi.org/10.1016/j.rser.2018.11.002.

Jamiolkowski, M., D. Lo Presti, and M. Manassero. 2003. "Evaluation of relative density and shear strength of sands from CPT and DMT." In *Soil Behavior and Soft Ground Construction, Geotechnical Special Publication 119*, 201–238. Reston, VA: ASCE.

Kallehave, D., B. W. Byrne, C. LeBlanc Thilsted, and K. K. Mikkelsen. 2015. "Optimization of monopiles for offshore wind turbines." *Philos. Trans. R. Soc. London, Ser. A* 373 (2035): 20140100. https://doi.org/10.1098/rsta.2014.0100.

Kementzetzidis, E., S. Corciulo, W. G. Versteijlen, and F. Pisanò. 2019. "Geotechnical aspects of offshore wind turbine dynamics from 3D nonlinear soil-structure simulations." *Soil Dyn. Earthquake Eng.* 120 (Jun): 181–199. https://doi.org/10.1016/j.soildyn.2019.01.037.

Kementzetzidis, E., A. V. Metrikine, W. G. Versteijlen, and F. Pisanò. 2021. "Frequency effects in the dynamic lateral stiffness of monopiles in sand: Insight from field tests and 3D FE modeling." *Géotechnique* 71 (9): 812–825. https://doi.org/10.1680/jgeot.19.TI.024.

Kementzetzidis, E., F. Pisanò, A. S. Elkadi, A. Tsouvalas, and A. V. Metrikine. 2023. "Gentle driving of piles (GDP) at a sandy site combining axial and torsional vibrations: Part II—Cyclic/dynamic lateral loading tests." *Ocean Eng.* 270 (Aug): 113452. https://doi.org/10.1016/j.oceaneng.2022.113452.

Kementzetzidis, E., F. Pisanò, and A. V. Metrikine. 2022. "A memory-enhanced model for piles in sand accounting for cyclic ratcheting and gapping effects." *Comput. Geotech.* 148 (Aug): 104810. https://doi.org/10.1016/j.compgeo.2022.104810.

Kementzetzidis, E., W. G. Versteijlen, A. Nernheim, and F. Pisanò. 2018. "3D FE dynamic modelling of offshore wind turbines in sand: Natural frequency evolution in the pre-to after-storm transition." In Vol. 2 of *Numerical methods in geotechnical engineering IX*, edited by A. S. Cardoso, J. L. Borges, P. A. Costa, A. T. Gomez, J. C. Marques, and C. S. Vieira, 1477–1484. Boca Raton, FL: CRC Press.

Komusanac, I., G. Brindley, D. Fraile, and R. Ramirez. 2022. *Wind energy in Europe: 2021 statistics and the outlook for 2022–2026*. Brussels, Belgium: WindEurope.

Labenski, J., and C. Moormann. 2019. "Lateral bearing behaviour of vibratory-driven monopiles: A modified py approach based on experimental observations of scaled model tests. Reykjavik, Iceland." In *Proc., 17th European Conf. on Soil Mechanics and Geotechnical Engineering*, edited by M. Hamza, M. Shahien, and Y. El-Mossallamy. Amsterdam, Netherlands: IOS Press BV.

LeBlanc, C. 2014. "Vibro-driving monopiles—A feasible installation concept for the future?" In Vol. 1 of *Proc., Danish Geotechnical Society Seminar*. Sapain, France: DocPlayer.

Lee, J., F. Zhao, and Dutton. 2021. *Global offshore wind report 2021*. Brussels, Belgium: Global Wind Energy Council.

Li, W., D. Igoe, and K. Gavin. 2015. "Field tests to investigate the cyclic response of monopiles in sand." *Proc. Inst. Civ. Eng. Geotech. Eng.* 168 (5): 407–421. https://doi.org/10.1680/jgeen.14.00104.

Liu, H., E. Kementzetzidis, J. A. Abell, and F. Pisanò. 2021. "From cyclic sand ratcheting to tilt accumulation of offshore monopiles: 3D FE modelling using SANISAND-MS." *Géotechnique* 72 (9): 753–768. https://doi.org/10.1680/jgeot.20.P.029.

Liu, H., F. Pisanò, H. P. Jostad, and N. Sivasithamparam. 2022. "Impact of cyclic strain accumulation on the tilting behaviour of monopiles in sand: An assessment of the Miner's rule based on SANISAND-MS 3D FE modeling." *Ocean Eng.* 250 (May): 110579. https://doi.org/10.1016/j.oceaneng.2022.110579.

Liu, H. Y., J. A. Abell, A. Diambra, and F. Pisanò. 2019. "Modelling the cyclic ratcheting of sands through memory-enhanced bounding surface plasticity." *Géotechnique* 69 (9): 783–800. https://doi.org/10.1680/jgeot.17.P.307.

Matlock, H., S. Foo, and L. Bryant. 1978. "Simulation of lateral pile behavior under earthquake motion." Vol. 1 of *Proc., ASCE Geotechnical Engineering Division Specialty Conf.*, 600–619. Reston, VA: ASCE.

McKenna, F. 2011. "OpenSees: A framework for earthquake engineering simulation." *Comput. Sci. Eng.* 13 (4): 58–66. https://doi.org/10.1109/MCSE.2011.66.

Metrikine, A., et al. 2020. "GDP: A new technology for Gentle Driving of (mono)Piles." In *Proc., 4th Int. Symp. on Frontiers in Offshore Geotechnics (ISFOG 2021), Frontiers in Offshore Geotechnics IV.*, edited by Z. Westgate, 736–745. Leiden, Netherlands: CRC Press.

Pisanò, F., A. Askarinejad, H. Wang, S. Maghsoodi, K. G. Gavin, M. L. A. Segeren, A. S. K. Elkadi, D. de Lange, and M. Konstadinou. 2022.

"MIDAS: Monopile improved design through advanced cyclic soil modelling." In *Proc., 20th Int. Conf. on Soil Mechanics and Geotechnical Engineering (ICSMGE2022)* St. Ives, NSW, Australia: Australian Geomechanics Society.

Prendergast, L., and D. Igoe. 2022. "Examination of the reduction in natural frequency of laterally loaded piles due to strain-dependence of soil shear modulus." *Ocean Eng.* 258 (Feb): 111614. https://doi.org/10.1016/j.oceaneng.2022.111614.

Prendergast, L. J., and K. Gavin. 2016. "A comparison of initial stiffness formulations for small-strain soil–pile dynamic Winkler modeling." *Soil Dyn. Earthquake Eng.* 81 (Mar): 27–41. https://doi.org/10.1016/j.soildyn.2015.11.006.

Randolph, M. F., and S. Gourvenec. 2011. *Offshore geotechnical engineering*. Oxford, UK: CRC Press.

Rodger, A., and G. Littlejohn. 1980. "A study of vibratory driving in granular soils." *Géotechnique* 30 (3): 269–293. https://doi.org/10.1680/geot.1980.30.3.269.

Staubach, P., J. Machaček, B. Bienen, and T. Wichtmann. 2022. "Long-term response of piles to cyclic lateral loading following vibratory and impact driving in water-saturated sand." *J. Geotech. Geoenviron. Eng.* 148 (11): 04022097. https://doi.org/10.1061/(ASCE)GT.1943-5606.0002906.

Staubach, P., J. Machaček, M. Moscoso, and T. Wichtmann. 2020. "Impact of the installation on the long-term cyclic behaviour of piles in sand: A numerical study." *Soil Dyn. Earthquake Eng.* 138 (Mar): 106223. https://doi.org/10.1016/j.soildyn.2020.106223.

Sturm, H., O. Solf, and P. Kudella. 2008. "Self-healing effects of shallow foundations for offshore wind turbine structures." In *Proc., 11th Baltic Sea Geotechnical Conf. on Geotechnics in Maritime Engineering*, edited by Z. Mlynarek, 301–308. London: CRC Press.

Suryasentana, S. K., and B. M. Lehane. 2014. "Numerical derivation of CPT-based p–y curves for piles in sand." *Géotechnique* 64 (3): 186–194. https://doi.org/10.1680/geot.13.P.026.

Suryasentana, S. K., and B. M. Lehane. 2016. "Updated CPT-based p–y formulation for laterally loaded piles in cohesionless soil under static loading." *Géotechnique* 66 (6): 445–453. https://doi.org/10.1680/jgeot.14.P.156.

Suzuki, Y., and S. Nakai. 1985. "Behavior of a pile under horizontal cyclic loading." In Vol. 3 of *Proc., 11th Int. Conf. on Soil Mechanics and Foundation Engineering*, 1413–1416. Rotterdam, Netherlands: A.A. Balkema.

Theodoros, T., K. Peter, and W. Torsten. 2009. "Geotechnical robustness and deformation recovery effects of offshore wind turbine foundations." In *Proc., 3rd Science Days on the Utilization of Offshore Wind Energy.* Oldenburg, Germany: Federal Ministry for the Environment.

Tsetas, A., et al. 2020. "Experimental identification of the dynamic behaviour of pile-soil system installed by means of three different pile-driving techniques." In Vol. II of *Proc., XI Int. Conf. on Structural Dynamics, EURODYN 2020*, edited by M. Papadrakakis, M. Fragiadakis, and C. Papadimitriou, 3005–3015. Bochum, Germany: European Association for Structural Dynamics.

Tsetas, A., A. Tsouvalas, S. S. Gómez, F. Pisanò, E. Kementzetzidis, T. Molenkamp, A. S. Elkadi, and A. V. Metrikine. 2023a. "Gentle driving of piles (GDP) at a sandy site combining axial and torsional vibrations: Part I—Installation tests." *Ocean Eng.* 270 (May): 113453. https://doi.org/10.1016/j.oceaneng.2022.113453.

Tsetas, A., A. Tsouvalas, and A. V. Metrikine. 2023b. "A non-linear three-dimensional pile–soil model for vibratory pile installation in layered media." *Int. J. Solids Struct.* 269 (Jun): 112202. https://doi.org/10.1016/j.ijsolstr.2023.112202.

Tsouvalas, A. 2020. "Underwater noise emission due to offshore pile installation: A review." *Energies* 13 (12): 3037. https://doi.org/10.3390/en13123037.

Wan, X., J. P. Doherty, and M. F. Randolph. 2021. "Relationships between lateral and rotational load transfer stiffnesses and soil modulus for the elastic response of monopoles." *Comput. Geotech.* 137 (Aug): 104256. https://doi.org/10.1016/j.compgeo.2021.104256.